




# Multi-Satellite Detection of Long-Range Transport and Transformation of Atmospheric Emissions from the Hunga Tonga-Hunga Ha'apai Volcano

Qinqin Liu <sup>1,2</sup>, Lu Gui <sup>3,\*</sup>, Jianqiang Liu <sup>4</sup> , Guido Ventura <sup>5</sup> , Qingzhou Yang <sup>3</sup>, Zhongting Wang <sup>6</sup>, Ziyue Tang <sup>3</sup>, Minghui Tao <sup>3</sup>  and Xuhui Shen <sup>1,2</sup>

- <sup>1</sup> State Key Laboratory of Space Weather, National Space Science Center, Chinese Academy of Sciences, No. 1 Zhongguancun Road, Beijing 100190, China; liuqinqin@nssc.ac.cn (Q.L.); shenxuhui@nssc.ac.cn (X.S.)
  - <sup>2</sup> Key Laboratory of Solar Activity and Space Weather, National Space Science Center, Chinese Academy of Sciences, No. 1 Zhongguancun Road, Beijing 100190, China
  - <sup>3</sup> Key Laboratory of Regional Ecology and Environmental Change, School of Geography and Information Engineering, China University of Geosciences, Wuhan 430074, China; caihonggeng21@mails.ucas.ac.cn (Q.Y.); zytang2000@cug.edu.cn (Z.T.); taomh@cug.edu.cn (M.T.)
  - <sup>4</sup> The Key Laboratory of Space Ocean Remote Sensing and Application, National Satellite Ocean Application Service, Ministry of Natural Resources, Beijing 100081, China; jqliu@mail.nsoas.org.cn
  - <sup>5</sup> Istituto Nazionale di Geofisica e Vulcanologia, Via di Vigna Murata, 605, 00143 Rome, Italy; guido.ventura@ingv.it
  - <sup>6</sup> Center for Satellite Application on Ecology and Environment, Ministry of Ecology and Environment, Beijing 100094, China; wangzt@secmep.cn
- \* Correspondence: guilu@cug.edu.cn; Tel.: +86-188-5219-2323



**Citation:** Liu, Q.; Gui, L.; Liu, J.; Ventura, G.; Yang, Q.; Wang, Z.; Tang, Z.; Tao, M.; Shen, X. Multi-Satellite Detection of Long-Range Transport and Transformation of Atmospheric Emissions from the Hunga Tonga-Hunga Ha'apai Volcano. *Remote Sens.* **2023**, *15*, 2661. <https://doi.org/10.3390/rs15102661>

Academic Editors: Tamas Várnai, Enrico Ferrero, Elvira Kovač-Andrić and Jonathan Procter

Received: 8 March 2023

Revised: 5 May 2023

Accepted: 18 May 2023

Published: 19 May 2023



**Copyright:** © 2023 by the authors. Licensee MDPI, Basel, Switzerland. This article is an open access article distributed under the terms and conditions of the Creative Commons Attribution (CC BY) license (<https://creativecommons.org/licenses/by/4.0/>).

**Abstract:** Large volumes of atmospheric pollutants injected into the troposphere and stratosphere from volcanic eruptions can exert significant influence on global climate. Through utilizing multi-satellite observations, we present a large-scale insight into the long-range transport and transformation of sulfur dioxide (SO<sub>2</sub>) emissions from the Hunga Tonga-Hunga Ha'apai eruption on 15 January 2022. We found that the transport of volcanic emissions, along with the transformation from SO<sub>2</sub> to sulfate aerosols, lasted for two months after the Tongan eruption. The emitted volume of SO<sub>2</sub> from the volcano eruption was approximately 183 kilotons (kt). Both satellite observation and numerical simulation results show that the SO<sub>2</sub> and volcanic ash plumes moved westward at a rate of one thousand kilometers per day across the Pacific and Atlantic Ocean regions and that SO<sub>2</sub> transformation in the atmosphere lasted for half a month. The transport and enhancement of aerosols is related to the conversion of SO<sub>2</sub> to sulfate. CALIPSO lidar observations show that SO<sub>2</sub> reached an altitude of 25–30 km and transformed into sulfate in the stratosphere after 29 January. Sulfate aerosols in the stratosphere deceased gradually with transport and fell back to the background level after two months. Our study shows that satellite observations give a good characterization of volcanic emissions, transport, and SO<sub>2</sub>-sulfate conversion, which can provide an essential constraint for climate modeling.

**Keywords:** Hunga Tonga-Hunga Ha'apai 2022 eruption; SO<sub>2</sub>; AOD; sulfate aerosol

## 1. Introduction

Eruptions of submarine volcanoes can affect atmospheric circulation and climate [1], producing temperature and rainfall anomalies, atmospheric pollution, ozone layer depletion, and acid rain. The rapid release of hot air, gases, and ash from volcanic eruptions into the upper troposphere and stratosphere can trigger wide environmental changes [2]. On 15 January 2022, a volcanic eruption occurred at Hunga Tonga-Hunga Ha'apai volcano in the Tonga-Kermadec subduction zone (Figure 1) [3]. The eruption lasted approximately 11 h, with an eruption column up to 58 km high [4,5]. This event generated a tsunami,

and gravity waves circled the Earth [6–8]. Poli and Shapiro [9] estimated a VEI (Volcanic Explosivity Index) of 6 for this event, which represents the largest submarine eruption ever recorded using geophysical instruments. Moreover, the Hunga volcano eruption injected a large amount of atmospheric pollutants into the troposphere and stratosphere.

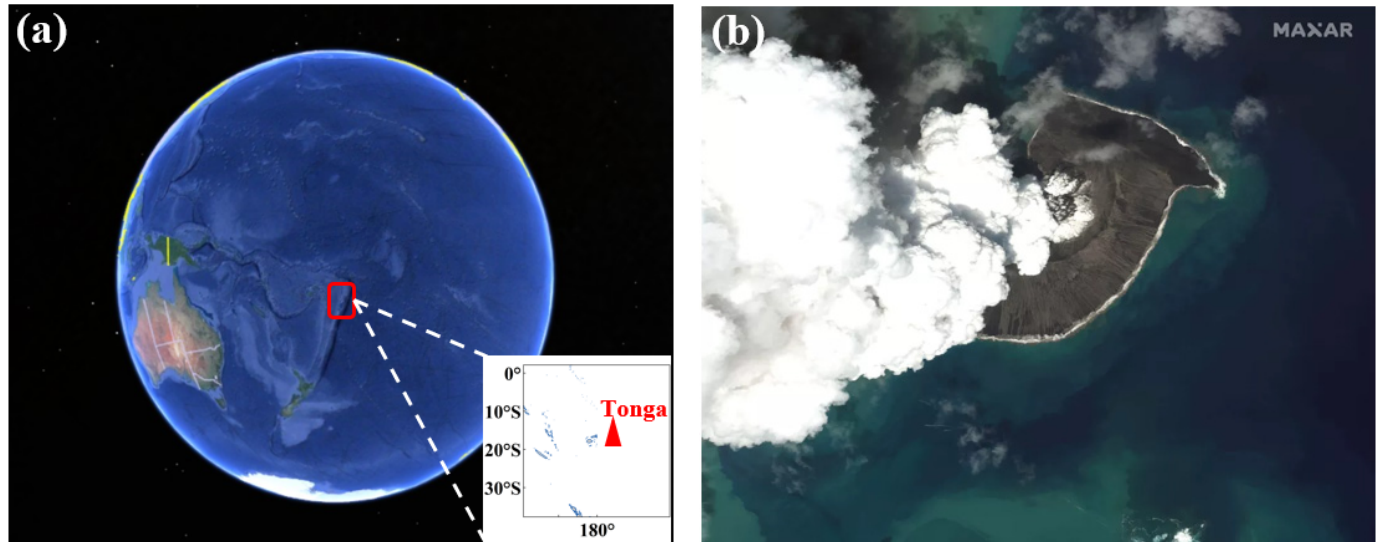


**Figure 1.** Location and photograph of Hunga-Tonga volcano. (a) Google geographical location (denoted by red triangle) and (b) photograph of Hunga-Tonga volcano. Image credit: Maxar Technologies.

Volcanic eruptions inject large amounts of sulfur-rich gases, mainly  $\text{SO}_2$  and sometimes  $\text{H}_2\text{S}$ , into the atmosphere, and the oxidation of these gases via OH and  $\text{H}_2\text{O}$  is a major pathway for the production of atmospheric sulfate aerosols, which take months or even years to settle to the Earth's surface. The lifetime of volcanic  $\text{SO}_2$  depends on its injection height,  $\text{SO}_2$  adherence on ash, and the concentrations of oxidants, which vary in space and time [10–12].  $\text{SO}_2$  from volcanic eruptions has a longer lifetime if it is injected into the stratosphere [13]. Sulfate aerosols play a crucial role in the climate through altering the radiation budget and cloud properties of the Earth–atmosphere system [14]. In particular, aerosols in the stratosphere strongly reflect solar radiation and reduce the solar radiation reaching the Earth, which results in a net cooling of the troposphere [15]. The large spatial and temporal variations of volcanic sulfate aerosols in the troposphere and stratosphere exert a challenge in quantifying their impacts on climate. The atmospheric emissions from the record-breaking Hunga volcano eruption and the transport of those emissions around the globe have not been well defined to date.

Satellite observations have been an indispensable tool for characterizing the spatial and temporal distribution of  $\text{SO}_2$  emissions from volcanoes worldwide [16]. Carn et al. [17] present a long-term record of  $\text{SO}_2$  emissions from 1978–1993 based on the TOMS satellite [17]. In the 2008 Kasatochi volcano eruption event, several infrared satellite sensors were used to detect  $\text{SO}_2$  emissions, including the Moderate-Resolution Imaging Spectroradiometer (MODIS), the Advanced Very-High-Resolution Radiometer (AVHRR), and the Atmospheric Infrared Sounder (AIRS) [18]. Understanding the dispersion of ash and  $\text{SO}_2$  produced by volcanic eruptions and their corresponding plumes is important, and Rix et al. [19] used the GOME-2 satellite instrument for observations of  $\text{SO}_2$  and BrO columns in the eruption plume and determination of  $\text{SO}_2$  plume heights. Because  $\text{SO}_2$  is a necessary input parameter for atmospheric chemistry and climate models, as it influences the spatial pattern of sulfate aerosols, the Ozone Monitoring Instrument (OMI) on NASA's Aura satellite gave an inventory of volcanic  $\text{SO}_2$  emissions [20,21]. The Tonga eruption in the southwest Pacific on 15 January 2022 triggered a large atmospheric disturbance [22–25], and the emissions of atmospheric pollutants from the eruption and the potential impact on climate are yet to be analyzed in detail.

In this study, we present a large-scale insight into the transport and transformation of the atmospheric emissions from the Tonga volcanic eruption on 15 January 2022 based on multi-satellite observations including TROPOMI (Tropospheric Monitoring Instrument), MODIS, and Cloud-Aerosol Lidar and Infrared Pathfinder Satellite Observation (CALIPSO) measurements. The height and lifetime of SO<sub>2</sub> injected into the atmosphere and the transformation process of SO<sub>2</sub> to sulfate aerosols in the stratosphere are analyzed. FLEXPART (Flexible Particle Diffusion Model) is used to simulate the diffusion process of SO<sub>2</sub> combined with meteorological data. The main purpose of our work is to provide a comprehensive perspective on how these volcanic emissions changed in the atmosphere along with their potential influence on climate.

## 2. Data and Method

### 2.1. TROPOMI

The TROPOMI instrument is an atmospheric multispectral sensor mounted on the Sentinel-5P satellite that records spectral reflectance. TROPOMI data report the atmospheric composition and other physical parameters through measuring the solar radiation reflected from the surface at the top of the atmosphere with the help of passive remote sensing techniques, mainly monitoring O<sub>3</sub>, SO<sub>2</sub>, NO<sub>2</sub>, HCHO, CO, CH<sub>4</sub>, clouds, aerosols, and other microphysical parameters [26]. TROPOMI operates in a push-and-sweep configuration with a strip width of about 2600 km at the Earth's surface and typical pixel sizes of 7 × 3.5 km for all spectral bands except the UV1 band (7 × 28 km) and the SWIR band (7 × 7 km) [27]. The operation of TROPOMI provides important information for the monitoring of volcanic and anthropogenic SO<sub>2</sub> emissions [28].

In particular, the SO<sub>2</sub> conversion equation is specified as

$$m = c \times M \times S, \quad (1)$$

where  $m$  is the total amount of SO<sub>2</sub> emissions,  $c$  is the SO<sub>2</sub> data from TROPOMI (mol/m<sup>2</sup>),  $M$  is the molar mass, and  $S$  is the emission area with higher TROPOMI SO<sub>2</sub> concentrations than background regions.

### 2.2. MODIS

The Moderate Resolution Imaging Spectroradiometer (MODIS) is carried onboard the Terra and Aqua satellites launched by NASA in 1999 and 2002, respectively. MODIS has a spatial resolution of 250 m–1000 m and a swath width of ~2330 km, and orbits at an altitude of 705 km. MODIS crosses the equator twice a day at about 10:30 a.m. and 1:30 p.m. local time. It detects the reflected and emitted radiation of the Earth using 36 bands between 0.4 and 14.0 µm, and it is capable of quantitative retrieval of global atmospheric parameters such as aerosols, clouds, and water vapor to monitor the process of natural hazards. The multispectral-based satellite sensor MODIS has the unique ability to invert aerosol optical thickness. MODIS aerosol inversion algorithms were developed over 20 years prior to the launch of the Terra satellite [29]. These algorithms were designed to take full advantage of the wide spectral range of the MODIS instrument. MODIS MOD/MYD04 550 nm AOD with a spatial resolution of 10 km is the most widely used global satellite aerosol. The Aqua MODIS C6 MYD08\_D3 and Terra MOD08\_D3 AOD products (tertiary aerosol products) with a combination of land and ocean 0.55 µm dark target and dark blue AOD average of daily averages were selected to analyze the transport of volcanic aerosol [30]. The dataset is presented on a Gaussian grid over the Earth's surface with a spatial resolution of 1° × 1°.

### 2.3. CALIPSO

The Cloud-Aerosol Lidar and Infrared Pathfinder Satellite Observation (CALIPSO) satellite was launched in April 2006 with a revisit period of 16 days. CALIPSO provides vertical detection of aerosols and clouds using 532 and 1064 nm lidar signals with a polarization measurement at 532 nm [31]. Despite the finer resolution, the Level 2 CALIPSO aerosol profile products are reported at a uniform horizontal resolution of 5 or 40 km

and a vertical resolution of 60–360 m to account for the weak backscattering signal from aerosols. The CALIPSO AOD for columnar extinction can be calculated via specifying the aerosol extinction-to-backscatter ratio (lidar ratio). Also, measurements of the attenuated backscatter and depolarization ratio can be used to identify the type of aerosols and clouds based on position, height, and surface types [32]. CALIPSO, in combination with other satellites in A-Train, can effectively detect the vertical structure and characteristics of clouds and aerosol layers [33]. Version V4.1 L2 CALIPSO aerosol products have been significantly improved in terms of extinction, optical depth [34], and aerosol classification [35]. CALIPSO provides an effective observational tool for monitoring stratospheric sulfate aerosols [36,37].

#### 2.4. AIRS

AIRS is carried onboard the EOS-Aqua satellite and was launched in May 2002 in polar orbit (1:30 pm ascent node). It is a hyperspectral instrument providing infrared coverage (<http://www-airs.jpl.nasa.gov>, accessed on 13 January 2022) at high spectral resolution ( $\lambda/\Delta\lambda = 1200$ ;  $\sim 0.5 \text{ cm}^{-1}$ ) from 649–1136, 1217–1613, and 2169–2674  $\text{cm}^{-1}$ . The scanning angle is  $\pm 49^\circ$  and the swath width is 1650 km. The spatial resolution is  $13.5 \times 13.5 \text{ km}^2$  at the bottom of the sky and the NE $\Delta$ T (noise equivalent change in temperature) is  $\sim 0.2 \text{ K}$  in the range 735–2674  $\text{cm}^{-1}$ . AIRS nominally observes the whole Earth (<http://www.airs.nasa.gov>, accessed on 13 January 2022) once during a 24 h period [18,38]. We select AIRS L2 surface air temperature and water vapor products to characterize the air changes during volcanic eruptions with a spatial resolution of  $0.5^\circ \times 0.5^\circ$ .

#### 2.5. FLEXPART Model

FLEXPART (Flexible Particle Diffusion Model) is a Lagrangian particle diffusion model [39] proved to be effective in simulating the transport of volcanic  $\text{SO}_2$  plumes [40]. This model has been widely used in a number of studies on long-range atmospheric transport [41–43]. The FLEXPART simulation requires five three-dimensional fields: horizontal wind U and V components, vertical wind W component, temperature, and humidity. FLEXPART also requires two-dimensional fields for the following parameters: ground pressure, total cloud cover, 10 m horizontal wind component, 2 m temperature and dew point temperature, large-scale convective precipitation, sensible heat flux, terrain height, land-sea identification, and sub-grid terrain standard deviation. The meteorological data for this simulation are in the Global Atmospheric Reanalysis dataset ds083.2, GRIB2 format, jointly developed by the National Centers for Environmental Prediction (NCEP) and the National Center for Atmospheric Research (NCAR). This dataset has global coverage, a spatial resolution of  $1^\circ \times 1^\circ$  grid, and vertical stratification of 26 standard pressure layers at 10 mb to 1000 mb heights. Forward simulations were carried out using the FLEXPART model, while grid concentration values and trajectory tracking results were output. <https://rda.ucar.edu/datasets/ds083.2/>, accessed on 14 January 2022. The relevant information of all satellite data used in the article is shown in Table 1.

**Table 1.** Details of the satellite products used.

Variables	Satellites	Instruments	Transit Time (BJT)	Resolution
AOD	Terra/Aqua	MODIS	10:30/13:30	10 km
$\text{SO}_2$	Sentinel-5P	TROPOMI	13:30	$7 \times 3.5 \text{ km}$
Total Attenuated Backscatter	CALIPSO	CALIOP	13:30	5 or 40 km (horizontal)/ 60–360 m (vertical)
Water Vapor/ Surface Air Temperature	Aqua	AIRS	13:30	50 km

### 3. Results

#### 3.1. Satellite Multi-Parameter Spatio-Temporal Tracking of Tonga Volcanic Eruption Process

The monitoring results of  $\text{SO}_2$  vertical column concentration by the TROPOMI satellite from 14 January to 27 January 2022 (Figure 2) show that the migration path of  $\text{SO}_2$  was



straight westward from the eruption of Hunga Tonga-Hunga Ha'apai volcano and mainly associated with a range of meteorological conditions that produced westerly winds transporting volcanic ash westwards (Figure S1). Temporal and spatial evolution results of the vertical column concentration of SO<sub>2</sub> from the volcano eruption are shown in Figure S2. On 16 January, the SO<sub>2</sub> plume migrated westward in the Pacific Ocean and gradually diffused. SO<sub>2</sub> reached Australia on 17 January while high SO<sub>2</sub> concentrations were still over the Pacific Ocean. The zone of high-concentration SO<sub>2</sub> stayed over the northern area of Australia on 18 and 19 January. The overall concentration of SO<sub>2</sub> decreased during 20 January and continued to move westward. On 21 January, SO<sub>2</sub> continued to spread westward and reached the Indian Ocean. On 22 January, the bulk SO<sub>2</sub> was torn into two parts. Meanwhile, the overall concentration of SO<sub>2</sub> decreased. After 23 January, SO<sub>2</sub> decreased significantly, until 27 January, and it almost disappeared.

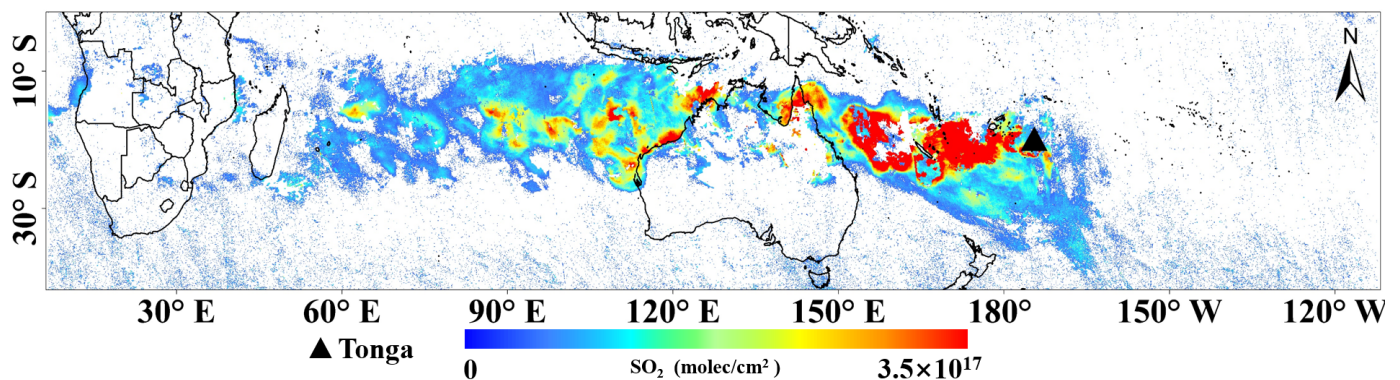


**Figure 2.** The transport path of SO<sub>2</sub> plumes from Tonga Volcano (black triangle) during 14–27 January 2022 with merged TROPOMI measurements.

The Hunga Tonga-Hunga Ha'apai undersea volcano erupted from 14 to 15 January 2022 [44], and the higher SO<sub>2</sub> concentrations mainly occurred in the vicinity of the vent. NASA estimated that the SO<sub>2</sub> concentrations and the coverage of SO<sub>2</sub> emissions associated with the eruption reached 58.48 kt on 14 January, and this manuscript estimates it reached 183 kt on 15 January, with an extent of 390,000 km<sup>2</sup> and 110,829 km<sup>2</sup>, respectively.

Figure 3 shows the results of the long-range spatial distribution of AOD for the period 14 January to 27 January 2022 from MODIS data. The high values of the spatial pattern of AOD started mainly in northern Australia and then extended to western South Africa. Some differences with the spatial pattern of SO<sub>2</sub> are shown in Figure 2. However, some similarity in the transport trajectories of SO<sub>2</sub> and AOD could be captured (Figures 2 and 3), which might also have an impact on the spatial pattern of AOD due to the frequent forest fires producing biomass-burning aerosols in Australia [45–47] and the frequent dust events in South Africa during the southern hemisphere summer [48–50]. We therefore could not directly conclude that the direct atmospheric conversion of volcanic eruption SO<sub>2</sub> formed sulfate aerosol distributed on a similar transport trajectory.

However, we further identify the conversion process of SO<sub>2</sub> to sulfate aerosols through CALIPSO lidar data, which is described in detail in Section 3.2. AOD spatial distribution results from MODIS data are shown in Figure S3. No obvious high AOD data were observed from 14 January to 16 January. On 17 January, there were some high AOD to the east of Australia. On the 18th, high AOD values were observed in northern Australia, and from the 19 to 21 January, the AOD plume migrated westward over the Indian Ocean. On 22 January, the AOD continued to move westward in southern Africa. On 23 January, some aerosols moved westward to the Atlantic Ocean, but the AOD high-value clusters remained in the southern African continent depicting a striped distribution. On the January 24, some aerosols continued to migrate westward and reached the southern part of the American continent. Some high-value AODs remained in the Atlantic region, and the strip-shaped area continued to expand. On 26 January, the AOD band-like area shrank and it mainly

distributed over southern Africa and the Atlantic Ocean. On 27 January, the AOD increased significantly in the southern region of the Americas and showed a slight upward trend in the Pacific Ocean, where the AOD increased significantly and continued to move westward.

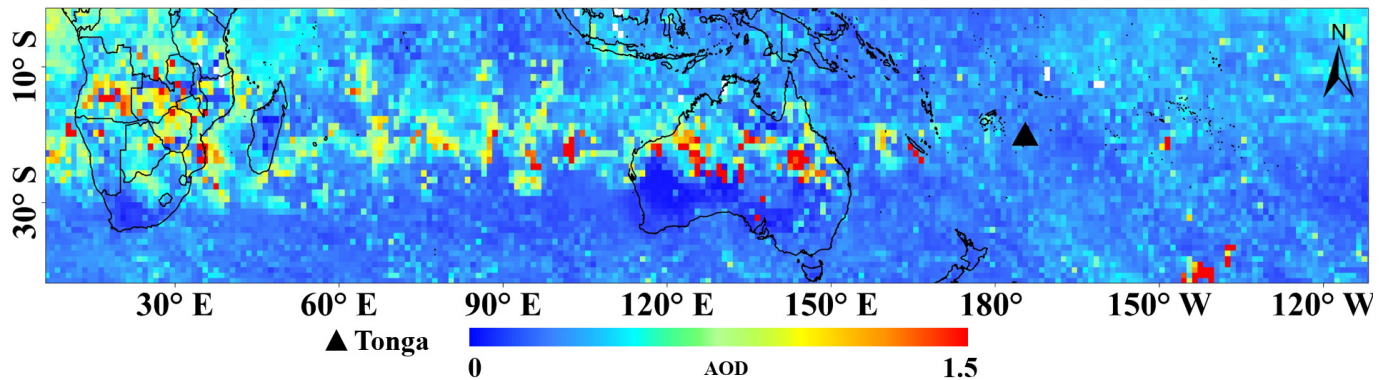


**Figure 3.** The long-range transport and transform of sulfate from Tonga Volcano (black triangle)  $\text{SO}_2$  with merged MODIS AOD during 14–27 January 2022.

The results of the spatial distribution of water vapor in the volcanic area of Tonga from 13–18 January 2022 (Figure 4) show a significant increase in water vapor concentrations around Hunga Tonga-Hunga Ha’apai at the time of the eruption on 14 January. It was also in an area of high values from 15–16 January, which began to decline on 17 January. The results of the spatial distribution of surface air temperatures around the vent from 13 January to 18 January 2022 (Figure 5) show a distribution of high surface temperatures across the area at the time of the eruption on 14 January. An abnormally high temperature near the surface of the volcano was also observed on 15 January. Surface temperatures returned to normal values on 17 January. Based on the AIRS satellite monitoring of water vapor and temperature changes, consistent with the  $\text{SO}_2$  eruption results, the volcano also produced changes in water vapor in addition to  $\text{SO}_2$  and  $\text{CO}_2$  [44,51,52].

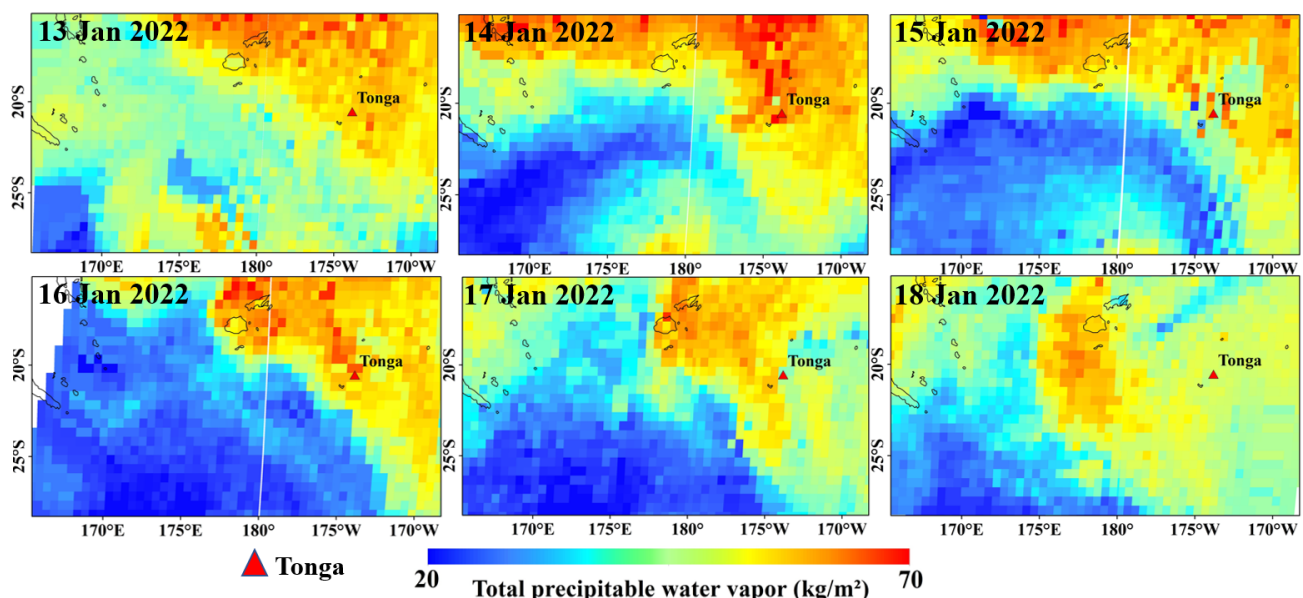


**Figure 4.** Spatial distribution of AIRS water vapor during 13–18 January 2022.



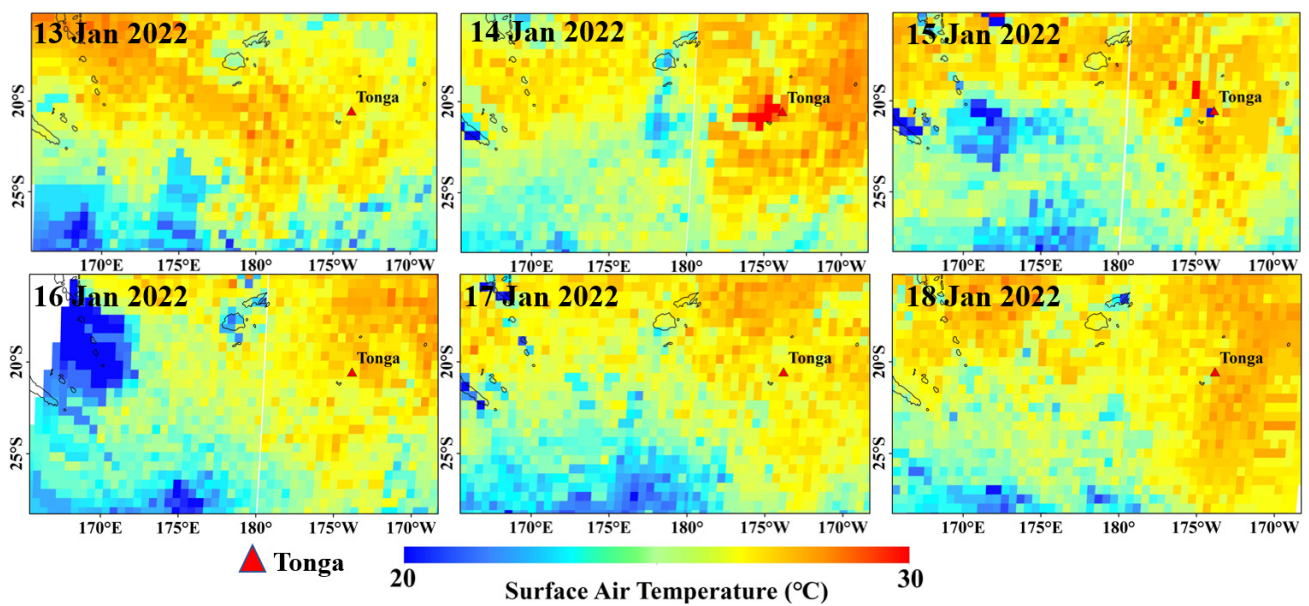


Figure 5. Spatial distribution of AIRS surface air temperature during 13–18 January 2022.

### 3.2. Sulfate Aerosol Plume Heights and Distribution

One focus of our study is the process of conversion of  $\text{SO}_2$  into sulfate aerosols during the Hunga Tonga-Hunga Ha'apai eruption. Figure 6 further shows that an obvious aerosol enhancement phenomenon appeared in the mid-latitude region of the Southern hemisphere from February to April through the difference results of the MODIS monthly data. In the stratosphere, volcanic sulfate aerosols may linger for months or even 1–3 years before fully dissipating, depending on  $\text{SO}_2$  injection altitude, total mass loading, latitude, and dispersion patterns [10,16,21].

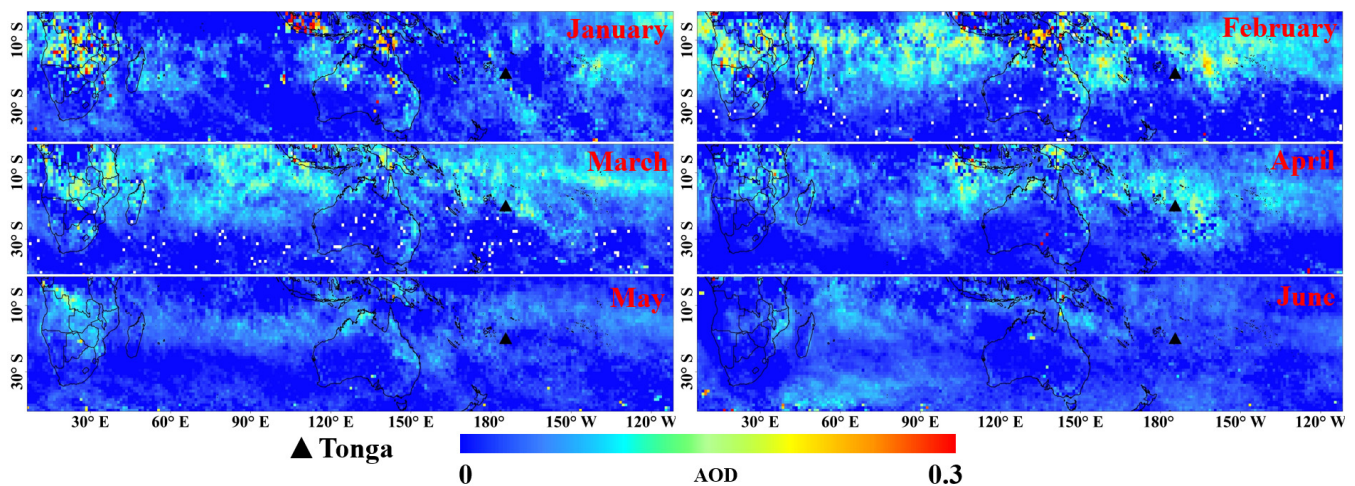


Figure 6. Monthly MODIS AOD difference 2022 vs. 2021.

Further identification of sulfate aerosols caused by the volcanic eruption requires the determination of the aerosol vertical height. CALIPSO provides vertical altitude observations for model simulations [53]. CALIPSO aerosol profiles provide a vertical view of the conversion of  $\text{SO}_2$  to sulfate after the ejection of  $\text{SO}_2$  aerosol into the atmosphere due to the eruption (Figure 7). On 16 January 2022, a strong extinction layer was captured at 25–30 km elevation near the vent. It appeared 25–30 km NE of Australia on 17 January 2022 and was transported to western Australia on 19 January 2022, with aerosol types mainly consisting of volcanic ash, sulfate, and aloft soot. CALIPSO shows the presence of

a strong extinction layer on 19 January 2022, yet the SO<sub>2</sub> concentration values are seen to be decreasing in Figure S2, while the AOD values are increasing in Figure S3. At the same time, it could be ruled out that biomass-burning aerosols from grassland and forest fires also formed transport strips (Figures 2 and 3). The conversion of SO<sub>2</sub> from the volcanic eruption into sulfate aerosols during transient transport is confirmed.

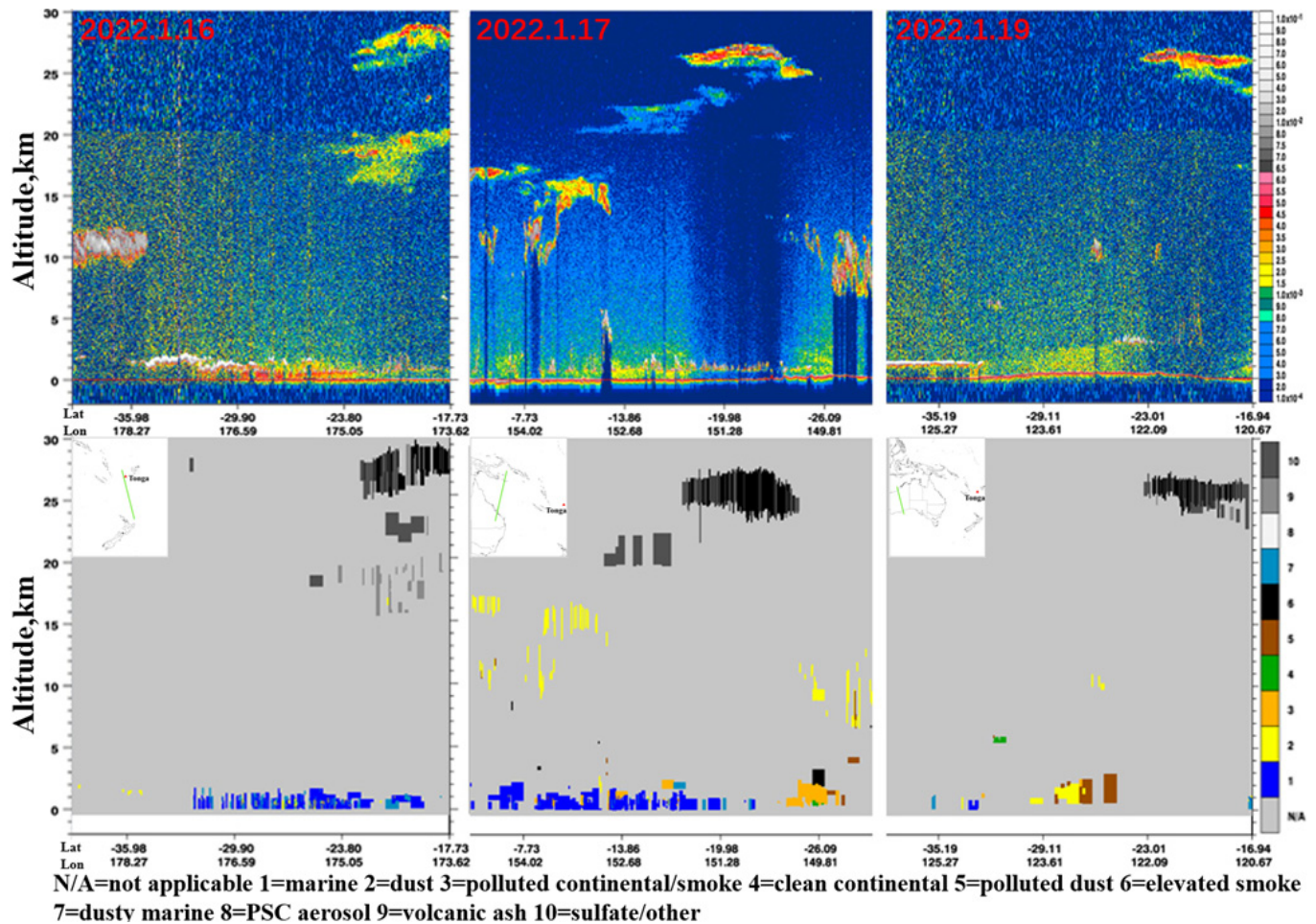


Figure 7. CALIPSO 523 nm total attenuated backscatter (top) and aerosol subtype (bottom).

The CALIPSO 532 nm attenuated backscatter for February 2022 and March 2022 is reported in Figures 8 and 9, and the transport trajectory in the upper right corner reveals that the eruption transported for at least two months in the Southern hemisphere, with a gradual decrease in extinction at 25 km in March 2022, consistent with the monthly data difference results between 2022 and 2021 of Figure 6.

### 3.3. Numerical Simulation of SO<sub>2</sub> Migration and Diffusion Process

We selected the air pollution diffusion model FLEXPART to simulate the SO<sub>2</sub> diffusion process from the Tonga volcanic eruption. Based on the TROPOMI satellite remote sensing data, the amount of SO<sub>2</sub> released by the eruption was ~183 kt. Release time is from 2022-01-15:0500 UTC to 2022-01-16:0500 UTC. Based on the vertical observation results of the CALIPSO satellite, the simulated SO<sub>2</sub> altitude ranges between 20~30 km, the simulated longitude range is from −180° to 180°, and the simulated latitude range is from 0° to 50°. The output grid concentration values and trajectory tracking results of the simulation are reported in Figure 10. These results show that the SO<sub>2</sub> released from eruption migrated to the west and the SO<sub>2</sub> concentration decreased gradually, accompanied by the SO<sub>2</sub> diffusion range increasing during the westward movement. The results of the FLEXPART model are consistent with the direction of dispersion of the volcanic plume simulated using



the TROPOMI satellite, reaching a maximum during 15–17 January 2022. This phase of maximum SO<sub>2</sub> concentration was followed by a gradual decrease on 18 January 2022 (Figure 2) and a regular increase in AOD values (Figure 3). On the basis of these data, we propose that the SO<sub>2</sub> cloud partially converted to sulfate aerosol in northern Australia (Figure S3). The comparison of the results from Figures S2 and S4 evidenced that the decreasing trend of diffusion concentration of SO<sub>2</sub> in the numerical simulation is not obvious between 23 and 27 January 2022, while SO<sub>2</sub> monitored via satellite remote sensing rapidly decreased at this time. This feature might be associated to the Figure S5 dry and wet deposition settings of SO<sub>2</sub> transformation mode in the FLEXPART model. In addition, numerical simulation results show that the migration path of SO<sub>2</sub> is consistent with the satellite observation, which is mainly related to the movement of the wind field in the stratosphere. The variation of the wind field extracted at the stratosphere height of about 20 km is reported in Figure S5, and the results evidence that the stratospheric wind field moved horizontally to the west within the range of  $-10^{\circ} \sim -30^{\circ}$ . The wind speed was about 10–20 m/s, a value consistent with the migration speed of SO<sub>2</sub>.

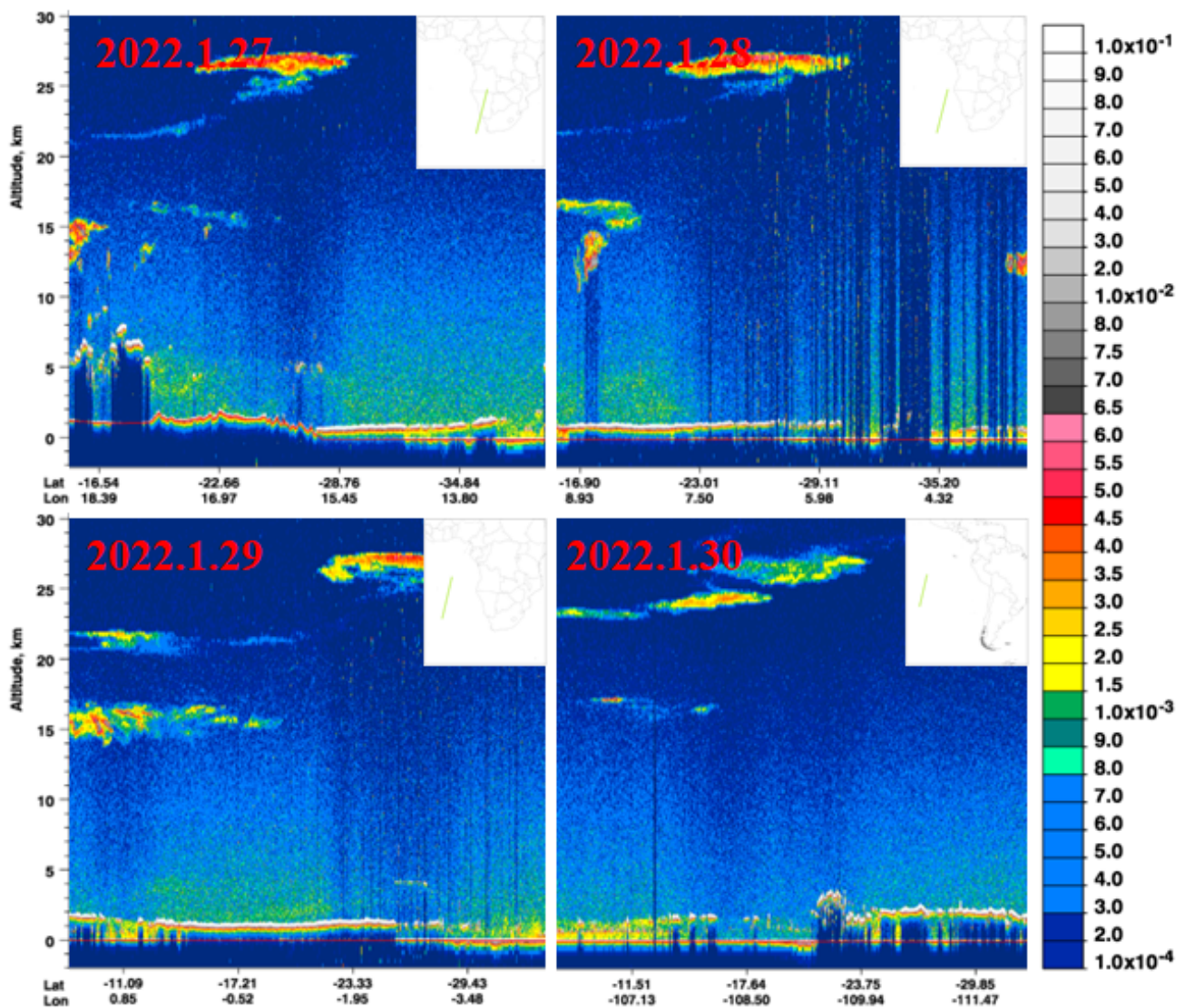


Figure 8. CALIPSO 523 nm total attenuation backscattering from 27 January 2022 to 31 January 2022.

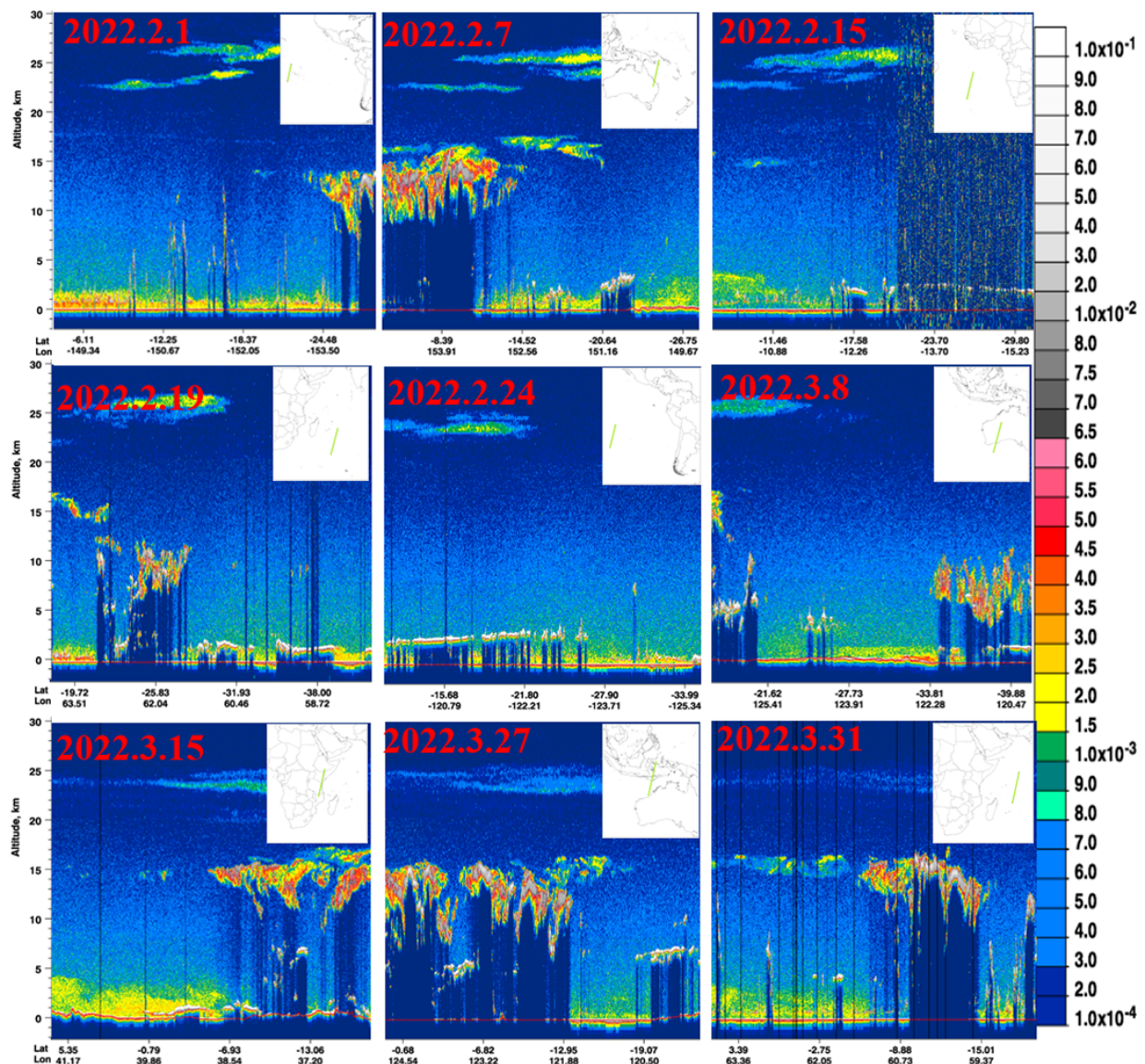


Figure 9. CALIPSO 523 nm total attenuation backscatter from February to March 2022.

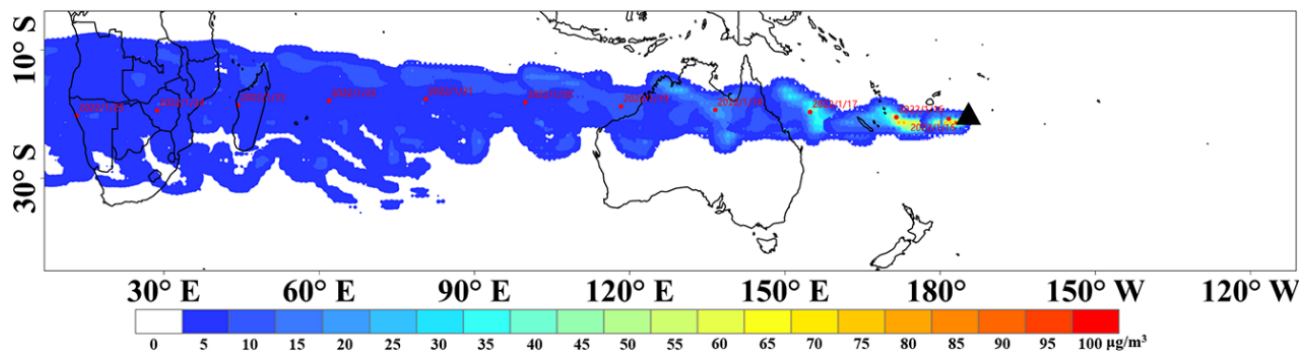


Figure 10. FLEXPART model simulates the transport of  $\text{SO}_2$  from 14 January 2022 to 25 January 2022.

#### 4. Discussion

Volcanic eruptions release variable amounts of ash and  $\text{SO}_2$  into the atmosphere and such  $\text{SO}_2$  may be converted to sulfate aerosols in a short period of time [54,55]. Stratospheric sulfate aerosols from volcanic eruptions can have lifetimes of 1–3 years and thus



have a relatively pronounced but irregular (or sporadic) impact on the chemistry of the atmosphere and effects on the Earth's radiative energy balance [16,56–58]. The surface air temperature well recorded high temperatures near the Hunga Tonga-Hunga Ha'apai vent on 14 and 15 January 2022, which may be related to the eruption. Previous studies report (a) a 5 km-wide ash column at 0530 UTC on 14 January (1830 local time; Global Volcanism Program (2022a)); (b) a plume rising to ~15 km of altitude with intermittent subaerial activity from 1143 to 1704 UTC on 14 January; (c) 10–15 min of eruption produced an ash plume that rose to 14 km at 1820 UTC on 14 January [6]; and (d) a plume that reached a maximum height of ~58 km, well within the mesosphere, at 0430 UTC on 15 January [59]. After the eruption, the ARIS satellite detected a significant increase in water vapor, which might be related to the water–magma interaction.

Our results show the dynamic dispersion of SO<sub>2</sub> moving westwards from the Pacific Ocean to Australia, the Indian Ocean, Africa, and the Atlantic Ocean at a rate of one thousand kilometers per day. With respect to the time period preceding 14 January 2022, the concentration of SO<sub>2</sub> increased by a factor of 30 during the eruption. The SO<sub>2</sub> released on 14 January was 58.48 kt, with the plume covering an area of ~390,000 km<sup>2</sup> (Figure S6). We estimate the SO<sub>2</sub> emitted during the eruption was about 183 kt according to the TROPOMI observation on 15 January 2022, (~0.2 Tg), consistent with Witze's [6] estimated SO<sub>2</sub> burden of 0.4–0.5 Tg. The SO<sub>2</sub> associated with the Hunga Tonga-Hunga Ha'apai eruption stayed in the atmosphere for about 2 weeks. Although the SO<sub>2</sub> removal mechanisms of wet and dry plumes remain poorly constrained in volcanic contexts [60,61], the injection height of SO<sub>2</sub> associated with the Hunga Tonga-Hunga Ha'apai eruption reached the stratosphere. In contrast to anthropogenic plumes, SO<sub>2</sub> lifetime is poorly constrained for tropospheric volcanic plumes, where the available loss rate estimates vary widely (from 1 to >99% per hour) [8]. In any case, the Hunga Tonga-Hunga Ha'apai eruption emitted a large amount of SO<sub>2</sub> reaching the stratosphere, which can explain its relatively long residence time.

After the volcanic eruption, AOD responded later than SO<sub>2</sub>, but its migration path was basically the same of SO<sub>2</sub>. The ejection height, migration, and diffusion of AOD and SO<sub>2</sub> occurred in the stratosphere (25–30 km), as confirmed using CALIPSO aerosol profiles and the direction of the wind field (Figure S5). It was reported by Kloss [62] that the Light Optical Aerosol Counter (LOAC) observations of a balloon flight on 23 January identified two main plume layers at around 22.6 and 24.9 km altitudes, consistent with the satellite monitoring results. The formation of AOD may be related to the SO<sub>2</sub> activity, and there might be some transformation correlation mechanism between AOD and SO<sub>2</sub>. Differently from SO<sub>2</sub>, AOD increased significantly in the African region where SO<sub>2</sub> gradually decreased and ultimately disappeared. Therefore, the production and transport of AOD can be related to the transformation of SO<sub>2</sub> into sulfate aerosols. Significant grassland, forest, and hill fires producing biomass-burning aerosols and dust aerosols from arid and semi-arid regions for long-range and large-scale transport between land and sea in mid to late January 2022 were lacking in Southern hemisphere land. Therefore, the recorded loss rate of SO<sub>2</sub> is indicative of the growth rate of sulfate aerosols [63]. Figures 2 and 3 show that both AOD and SO<sub>2</sub> expanded gradually. After the eruption, SO<sub>2</sub> gradually decreased in the westward migration process, but, in the Atlantic region, AOD expansion was significantly higher than SO<sub>2</sub>. After 27 January, the SO<sub>2</sub> was almost removed, but AOD still remained in the atmosphere and continued to propagate westward.

Based on the aerosol vertical profile from CALIPSO, a strong extinction layer was captured at 25–30 km of altitude (the aerosol type is mainly volcanic ash). It could be ruled out that biomass-burning aerosols from grassland and forest fires also formed transport belts. In fact, volcanic eruptions should reach much higher altitudes [59,64]. As a result, the conversion of SO<sub>2</sub> from the volcanic eruption into sulfate aerosols during transient transport is confirmed. At the same time, particles with radii between 0.5 and 1.0 µm show optically transparent features pointing to predominant sulfate aerosols [62], which further proves the fact that SO<sub>2</sub> was converted to sulfate aerosols during the migration. Figure 9 shows the CALIPSO 532 nm backscattered extinction coefficient for February

2022–March 2022. Sulfate-type aerosols were mainly distributed in the stratospheric region at the height of 25–30 km, and the thickness of sulfate-type aerosols gradually thinned over time: the thickness of stratospheric aerosols is slightly visible in the vertical observation on 31 March 2022. Compared with SO<sub>2</sub>, AOD has a longer survival time in the atmosphere and a longer potential impact on the environment. It was reported that effective lifetimes of volcanic SO<sub>2</sub> plumes could last for 43–61 h between 1.10–2.73 km of altitude. These values are consistent with those predicted by Beirle et al. [65] and GEOS-Chem [63]. Although volcanoes may directly release aerosols, however, large amounts of SO<sub>2</sub> could also generate sulfate aerosols, as in the case of the of the Hunga Tonga-Hunga Ha’apai eruption, which was also accompanied by large amounts of vapor. On the basis of our numerical simulations, the volcanic SO<sub>2</sub> released during the 15 January 2022 eruption reached the stratosphere and its diffusion trend and path were mainly controlled by the wind field. The comparison between the results of the numerical simulations and the satellite observations indicated that, after the eruption, the stratospheric environment allowed the removal of SO<sub>2</sub>.

## 5. Conclusions

We provide a comprehensive insight into the long-range transport and transformation process of the atmospheric emissions from the 2022 Hunga Tonga-Hunga Ha’apai volcano eruption through combining satellite data and numeral simulation results. TROPOMI, MODIS, AIRS, and CALIPSO satellite data recorded substantial spatial variations of SO<sub>2</sub>, AOD, water vapor, and surface temperature caused by the volcano’s eruption. Our results show an increase of the surface temperature on 14 January 2022. The released amount of SO<sub>2</sub> is ~183 kt and a rough estimate of the dynamic dispersion of SO<sub>2</sub> is in the order of tens of thousands of miles with a rate of one thousand kilometers per day. SO<sub>2</sub> crossed the Pacific Ocean, Australia, the Indian Ocean, Africa, and the Atlantic Ocean and remained in the atmosphere for half a month before dissipating in the Atlantic Ocean. Interestingly, the aerosol loading increased significantly in the Atlantic Ocean with the decrease of SO<sub>2</sub>, which is due to the formation of sulfate aerosols. CALIPSO detected that the SO<sub>2</sub> released by the eruption reached altitudes of 25–30 km and was converted to sulfate aerosols. Sulfate aerosols stayed in the stratosphere for more than two months after the eruption, and were mainly concentrated in the middle and lower latitudes of the Southern hemisphere. Compared to the residence time of SO<sub>2</sub>, the sulfate aerosols have a longer residence time in the atmosphere and spread over a wider area. According to the SO<sub>2</sub> injection height and amount observed using TROPOMI and CALIPSO satellites, FLEXPART model simulations show that the transport and diffusion process of volcanic SO<sub>2</sub> is dependent on the westward wind field from the stratosphere.

**Supplementary Materials:** The following supporting information can be downloaded at: <https://www.mdpi.com/article/10.3390/rs15102661/s1>, Figure S1: 72-h forward and backward trajectory maps for the Tonga volcanic event during 22 January and 27 January 2022, at 10 km, 20 km and 25 km; Figure S2: Temporal and spatial evolution results of vertical column concentration of SO<sub>2</sub> in Tonga volcano. The black triangle represents the location of the Hunga Tonga-Hunga Ha’apai volcano; Figure S3: AOD spatial distribution results from 14 January to 27 January 2022. The black triangle represents the location of the Hunga Tonga-Hunga Ha’apai volcano. The data source is MODIS, which is the same as Figure 3; Figure S4: Spatio-temporal evolution results of SO<sub>2</sub> numerical simulation from 15 January to 27 January 2022; Figure S5: Stratospheric wind field at about 20 km (Unit, m/s); Figure S6: SO<sub>2</sub> concentration values on January 14 around the satellite around the outburst from NASA website. (<https://SO2.gsfc.nasa.gov>, accessed on 14 January 2022.).

**Author Contributions:** Q.L.: conceptualization, methodology, validation, writing—original draft, and writing—review and editing. L.G.: software, investigation, formal analysis, writing—original draft, and writing—review and editing. J.L.: investigation, formal analysis, and methodology. G.V.: writing—review and editing and supervision. M.T.: formal analysis and conceptualization. Q.Y.: software, investigation, and project administration. Z.W.: software and formal analysis. Z.T.: writing—review & editing. X.S.: formal analysis and conceptualization. All authors have read and agreed to the published version of the manuscript.



**Funding:** This work was supported by the State Administration of Science, Technology and Industry for National Defence, PRC No. KJSP2020020303, China National Space Administration Preliminary Research Project KJSP2020020101, the National Natural Science Foundation of China (Grant No. 42203082), Project No. E3RC2TQ5, and Project No. E3RC2TQ4.

**Data Availability Statement:** The data presented in this study are available in insert article.

**Acknowledgments:** We wish to acknowledge State Key Laboratory of Space Weather, National Space Science Center, Chinese Academy of Sciences, School of Geography and Information Engineering, China University of Geosciences, the Istituto Nazionale di Geofisica e Vulcanologia (INGV), and the Center for Satellite Application on Ecology and Environment for giving us the chance of cooperation. Qinqin Liu organized and co-wrote the manuscript after the Tonga volcano eruption. Thanks to Lu Gui, Qingzhou Yang, and Minghui Tao for the help about some data processing. Thanks to the research proposal of Xuhui Shen, Jianqiang Liu, Minghui Tao, and Zhongting Wang. Thanks to Jianqiang Liu, Guido Ventura, and Ziyue Tang for revising the manuscript, and thanks for the support from the State Key Laboratory of Space Weather, National Space Science Center, Chinese Academy of Sciences.

**Conflicts of Interest:** The authors declare that they have no known competing financial interest or personal relationship that could have appeared to influence the work reported in this paper.

## References

- Ernst, G.; Kervyn, M.; Teeuw, R. Advances in the remote sensing of volcanic activity and hazards, with special consideration to applications in developing countries. *Int. J. Remote Sens.* **2008**, *29*, 6687–6723. [\[CrossRef\]](#)
- Adam, D. Tonga volcano created puzzling atmospheric ripples. *Nature* **2022**, *602*, 2022.
- Chen, C.-H.; Zhang, X.; Sun, Y.-Y.; Wang, F.; Liu, T.-C.; Lin, C.-Y.; Gao, Y.; Lyu, J.; Jin, X.; Zhao, X. Individual Wave Propagations in Ionosphere and Troposphere Triggered by the Hunga Tonga-Hunga Ha’apai Underwater Volcano Eruption on 15 January 2022. *Remote Sens.* **2022**, *14*, 2179. [\[CrossRef\]](#)
- Duncombe, J. The surprising reach of Tonga’s giant atmospheric waves. *Eos* **2022**, *103*, 1029. [\[CrossRef\]](#)
- Kusky, T.M. Déjà vu: Might Future Eruptions of Hunga Tonga-Hunga Ha’apai Volcano be a Repeat of the Devastating Eruption of Santorini, Greece (1650 BC)? *J. Earth Sci.* **2022**, *33*, 229–235. [\[CrossRef\]](#)
- Terry, J.P.; Goff, J.; Winspear, N.; Bongolan, V.P.; Fisher, S. Tonga volcanic eruption and tsunami, January 2022: Globally the most significant opportunity to observe an explosive and tsunamigenic submarine eruption since AD 1883 Krakatau. *Geosci. Lett.* **2022**, *9*, 24. [\[CrossRef\]](#)
- Vergoz, J.; Hupe, P.; Listowski, C.; Le Pichon, A.; Garcés, M.A.; Marchetti, E.; Labazuy, P.; Ceranna, L.; Pilger, C.; Gaebler, P.; et al. IMS observations of infrasound and acoustic-gravity waves produced by the January 2022 volcanic eruption of Hunga, Tonga: A global analysis. *Earth Planet. Sci. Lett.* **2022**, *591*, 117639. [\[CrossRef\]](#)
- Witze, A. Why the Tongan eruption will go down in the history of volcanology. *Nature* **2022**, *602*, 376–378. [\[CrossRef\]](#)
- Poli, P.; Shapiro, N.M. Rapid characterization of large volcanic eruptions: Measuring the impulse of the Hunga Tonga Ha’apai explosion from teleseismic waves. *Geophys. Res. Lett.* **2022**, *49*, e2022GL098123. [\[CrossRef\]](#)
- Krotkov, N.A.; Schoeberl, M.; Morris, G.; Carn, S.; Yang, K. Dispersion and lifetime of the SO<sub>2</sub> cloud from the August 2008 Kasatochi eruption. *J. Geophys. Res. Atmos.* **2010**, *115*, D2. [\[CrossRef\]](#)
- Beirle, S.; Hörmann, C.; de Vries, M.P.; Dörner, S.; Kern, C.; Wagner, T. Estimating the volcanic emission rate and atmospheric lifetime of SO<sub>2</sub> from space: A case study for Kīlauea volcano, Hawai’i. *Atmos. Chem. Phys.* **2014**, *14*, 8309–8322. [\[CrossRef\]](#)
- Gorkavyi, N.; Krotkov, N.; Li, C.; Lait, L.; Colarco, P.; Carn, S.; DeLand, M.; Newman, P.; Schoeberl, M.; Taha, G.; et al. Tracking aerosols and SO<sub>2</sub> clouds from the Raikoke eruption: 3D view from satellite observations. *Atmos. Meas. Technol.* **2021**, *14*, 7545–7563. [\[CrossRef\]](#)
- Carn, S.A.; Clarisse, L.; Prata, A.J. Multi-decadal satellite measurements of global volcanic degassing. *J. Volcanol. Geotherm. Res.* **2016**, *311*, 99–134. [\[CrossRef\]](#)
- Hansen, J.E.; Wang, W.-C.; Lacis, A.A. Mount Agung eruption provides test of a global climatic perturbation. *Science* **1978**, *199*, 1065–1068. [\[CrossRef\]](#) [\[PubMed\]](#)
- Brodowsky, C.; Sukhodolov, T.; Feinberg, A.; Höpfner, M.; Peter, T.; Stenke, A.; Rozanov, E. Modeling the sulfate aerosol evolution after recent moderate volcanic activity, 2008–2012. *J. Geophys. Res. Atmos.* **2021**, *126*, e2021JD035472. [\[CrossRef\]](#)
- Wang, J.; Park, S.; Zeng, J.; Ge, C.; Yang, K.; Carn, S.; Krotkov, N. Omar. Modeling of 2008 Kasatochi volcanic sulfate direct radiative forcing: Assimilation of OMI SO<sub>2</sub> plume height data and comparison with MODIS and CALIOP observations. *Atmos. Chem. Phys.* **2013**, *13*, 1895–1912. [\[CrossRef\]](#)
- Carn, S.; Krueger, A.; Bluth, G.; Schaefer, S.; Krotkov, N.; Watson, I.; Datta, S. Volcanic eruption detection by the Total Ozone Mapping Spectrometer (TOMS) instruments: A 22-year record of sulphur dioxide and ash emissions. *Geol. Soc. Lond. Spec. Publ.* **2003**, *213*, 177–202. [\[CrossRef\]](#)

18. Corradini, S.; Merucci, L.; Prata, A.; Piscini, A. Volcanic ash and SO<sub>2</sub> in the 2008 Kasatochi eruption: Retrievals comparison from different IR satellite sensors. *J. Geophys. Res. Atmos.* **2010**, *115*, D2. [[CrossRef](#)]
19. Rix, M.; Valks, P.; Hao, N.; Loyola, D.; Schlager, H.; Huntrieser, H.; Flemming, J.; Koehler, U.; Schumann, U.; Inness, A. Volcanic SO<sub>2</sub>, BrO and plume height estimations using GOME-2 satellite measurements during the eruption of Eyjafjallajökull in May 2010. *J. Geophys. Res. Atmos.* **2012**, *117*, D20. [[CrossRef](#)]
20. Carn, S.; Fioletov, V.; McLinden, C.; Li, C.; Krotkov, N. A decade of global volcanic SO<sub>2</sub> emissions measured from space. *Sci. Rep.* **2017**, *7*, 44095. [[CrossRef](#)]
21. Ge, C.; Wang, J.; Carn, S.; Yang, K.; Ginoux, P.; Krotkov, N. Satellite-based global volcanic SO<sub>2</sub> emissions and sulfate direct radiative forcing during 2005–2012. *J. Geophys. Res. Atmos.* **2016**, *121*, 3446–3464. [[CrossRef](#)]
22. Themens, D.R.; Watson, C.; Žagar, N.; Vasylyevych, S.; Elvidge, S.; McCaffrey, A.; Prikryl, P.; Reid, B.; Wood, A.; Jayachandran, P. Global propagation of ionospheric disturbances associated with the 2022 Tonga Volcanic Eruption. *Geophys. Res. Lett.* **2022**, *49*, e2022GL098158. [[CrossRef](#)]
23. Aa, E.; Zhang, S.R.; Wang, W.; Erickson, P.J.; Qian, L.; Eastes, R.; Harding, B.J.; Immel, T.J.; Karan, D.K.; Daniell, R.E. Pronounced suppression and X-pattern merging of equatorial ionization anomalies after the 2022 Tonga volcano eruption. *J. Geophys. Res. Space Phys.* **2022**, *127*, e2022JA030527. [[CrossRef](#)] [[PubMed](#)]
24. Lin, J.T.; Rajesh, P.K.; Lin, C.C.; Chou, M.Y.; Liu, J.Y.; Yue, J.; Hsiao, T.Y.; Tsai, H.F.; Chao, H.M.; Kung, M.M. Rapid Conjugate Appearance of the Giant Ionospheric Lamb Wave Signatures in the Northern Hemisphere After Hunga-Tonga Volcano Eruptions. *Geophys. Res. Lett.* **2022**, *49*, e2022GL098222. [[CrossRef](#)]
25. Liu, X.; Xu, J.; Yue, J.; Kogure, M. Strong Gravity Waves associated with Tonga Volcano Eruption Revealed by SABER Observations. *Geophys. Res. Lett.* **2022**, *49*, 10. [[CrossRef](#)]
26. Veeffkind, J.; Aben, I.; McMullan, K.; Förster, H.; De Vries, J.; Otter, G.; Claas, J.; Eskes, H.; De Haan, J.; Kleipool, Q. TROPOMI on the ESA Sentinel-5 Precursor: A GMES mission for global observations of the atmospheric composition for climate, air quality and ozone layer applications. *Remote Sens. Environ.* **2012**, *120*, 70–83. [[CrossRef](#)]
27. Theys, N.; De Smedt, I.; Yu, H.; Danckaert, T.; van Gent, J.; Hörmann, C.; Wagner, T.; Hedelt, P.; Bauer, H.; Romahn, F.; et al. Sulfur dioxide retrievals from TROPOMI onboard Sentinel-5 Precursor: Algorithm theoretical basis. *Atmos. Meas. Tech.* **2017**, *10*, 119–153. [[CrossRef](#)]
28. Burton, M.; Hayer, C.; Miller, C.; Christenson, B. Insights into the 9 December 2019 eruption of Whakaari/White Island from analysis of TROPOMI SO<sub>2</sub> imagery. *Sci. Adv.* **2021**, *7*, eabg1218. [[CrossRef](#)]
29. Levy, R.; Mattoo, S.; Munchak, L.; Remer, L.; Sayer, A.; Patadia, F.; Hsu, N. The Collection 6 MODIS aerosol products over land and ocean. *Atmos. Meas. Tech.* **2013**, *6*, 2989–3034. [[CrossRef](#)]
30. Bright, J.M.; Gueymard, C.A. Climate-specific and global validation of MODIS Aqua and Terra aerosol optical depth at 452 AERONET stations. *Sol. Energy* **2019**, *183*, 594–605. [[CrossRef](#)]
31. Liu, Z.; Liu, D.; Huang, J.; Vaughan, M.; Uno, I.; Sugimoto, N.; Kittaka, C.; Trepte, C.; Wang, Z.; Hostetler, C. Airborne dust distributions over the Tibetan Plateau and surrounding areas derived from the first year of CALIPSO lidar observations. *Atmos. Chem. Phys.* **2008**, *8*, 5045–5060. [[CrossRef](#)]
32. Omar, A.H.; Winker, D.M.; Vaughan, M.A.; Hu, Y.; Trepte, C.R.; Ferrare, R.A.; Lee, K.-P.; Hostetler, C.A.; Kittaka, C.; Rogers, R.R. The CALIPSO automated aerosol classification and lidar ratio selection algorithm. *J. Atmos. Ocean. Technol.* **2009**, *26*, 1994–2014. [[CrossRef](#)]
33. Gui, L.; Tao, M.; Wang, Y.; Wang, L.; Chen, L.; Lin, C.; Tao, J.; Wang, J.; Yu, C. Climatology of aerosol types and their vertical distribution over East Asia based on CALIPSO lidar measurements. *Int. J. Climatol.* **2022**, *42*, 6042–6054. [[CrossRef](#)]
34. Young, S.A.; Vaughan, M.A.; Garnier, A.; Tackett, J.L.; Lambeth, J.D.; Powell, K.A. Extinction and optical depth retrievals for CALIPSO's Version 4 data release. *Atmos. Meas. Tech.* **2018**, *11*, 5701–5727. [[CrossRef](#)]
35. Kim, M.-H.; Omar, A.H.; Tackett, J.L.; Vaughan, M.A.; Winker, D.M.; Trepte, C.R.; Hu, Y.; Liu, Z.; Poole, L.R.; Pitts, M.C. The CALIPSO version 4 automated aerosol classification and lidar ratio selection algorithm. *Atmos. Meas. Tech.* **2018**, *11*, 6107–6135. [[CrossRef](#)]
36. Vernier, J.-P.; Pommereau, J.-P.; Garnier, A.; Pelon, J.; Larsen, N.; Nielsen, J.; Christensen, T.; Cairo, F.; Thomason, L.W.; Leblanc, T. Tropical stratospheric aerosol layer from CALIPSO lidar observations. *J. Geophys. Res. Atmos.* **2009**, *114*, D4. [[CrossRef](#)]
37. Kovilakam, M.; Thomason, L.W.; Ernest, N.; Rieger, L.; Bourassa, A.; Millán, L. The global space-based stratospheric aerosol climatology (version 2.0): 1979–2018. *Earth Syst. Sci. Data* **2020**, *12*, 2607–2634. [[CrossRef](#)]
38. Carn, S.; Strow, L.D.; de Souza-Machado, S.; Edmonds, Y.; Hannon, S. Quantifying tropospheric volcanic emissions with AIRS: The 2002 eruption of Mt. Etna (Italy). *Geophys. Res. Lett.* **2005**, *32*, 2. [[CrossRef](#)]
39. Renuka, K.; Gadhavi, H.; Jayaraman, A.; Rao, S.; Lal, S. Study of mixing ratios of SO<sub>2</sub> in a tropical rural environment in south India. *J. Earth Syst. Sci.* **2020**, *129*, 104. [[CrossRef](#)]
40. Stohl, A.; Hittenberger, M.; Wotawa, G. Validation of the Lagrangian particle dispersion model FLEXPART against large-scale tracer experiment data. *Atmos. Environ.* **1998**, *32*, 4245–4264. [[CrossRef](#)]
41. Fiedler, V.; Nau, R.; Ludmann, S.; Arnold, F.; Schlager, H.; Stohl, A. East Asian SO<sub>2</sub> pollution plume over Europe—Part 1: Airborne trace gas measurements and source identification by particle dispersion model simulations. *Atmos. Chem. Phys.* **2009**, *9*, 4717–4728. [[CrossRef](#)]

42. Damoah, R.; Spichtinger, N.; Forster, C.; James, P.; Mattis, I.; Wandinger, U.; Beirle, S.; Wagner, T.; Stohl, A. Around the world in 17 days-hemispheric-scale transport of forest fire smoke from Russia in May 2003. *Atmos. Chem. Phys.* **2004**, *4*, 1311–1321. [\[CrossRef\]](#)
43. Eckhardt, S.; Breivik, K.; Manø, S.; Stohl, A. Record high peaks in PCB concentrations in the Arctic atmosphere due to long-range transport of biomass burning emissions. *Atmos. Chem. Phys.* **2007**, *7*, 4527–4536. [\[CrossRef\]](#)
44. Zhang, H.; Wang, F.; Li, J.; Duan, Y.; Zhu, C.; He, J. *Potential Impact of Tonga Volcano Eruption on Global Mean Surface Air Temperature*; Springer: Berlin/Heidelberg, Germany, 2022.
45. Chang, D.Y.; Yoon, J.; Lelieveld, J.; Park, S.K.; Yum, S.S.; Kim, J.; Jeong, S. Direct radiative forcing of biomass burning aerosols from the extensive Australian wildfires in 2019–2020. *Environ. Res. Lett.* **2021**, *16*, 044041. [\[CrossRef\]](#)
46. Keywood, M.; Kanakidou, M.; Stohl, A.; Dentener, F.; Grassi, G.; Meyer, C.; Torseth, K.; Edwards, D.; Thompson, A.M.; Lohmann, U. Fire in the air: Biomass burning impacts in a changing climate. *Crit. Rev. Environ. Sci. Technol.* **2013**, *43*, 40–83. [\[CrossRef\]](#)
47. Mallet, M.D.; Desservettaz, M.J.; Miljevic, B.; Milic, A.; Ristovski, Z.D.; Alroe, J.; Cravigan, L.T.; Jayaratne, E.R.; Paton-Walsh, C.; Griffith, D.W. Biomass burning emissions in north Australia during the early dry season: An overview of the 2014 SAFIRED campaign. *Atmos. Chem. Phys.* **2017**, *17*, 13681–13697. [\[CrossRef\]](#)
48. Hersey, S.P.; Garland, R.M.; Crosbie, E.; Shingler, T.; Sorooshian, A.; Piketh, S.; Burger, R. An overview of regional and local characteristics of aerosols in South Africa using satellite, ground, and modeling data. *Atmos. Chem. Phys.* **2015**, *15*, 4259–4278. [\[CrossRef\]](#)
49. Tanaka, T.Y.; Chiba, M. A numerical study of the contributions of dust source regions to the global dust budget. *Glob. Planet. Chang.* **2006**, *52*, 88–104. [\[CrossRef\]](#)
50. Ginoux, P.; Chin, M.; Tegen, I.; Prospero, J.M.; Holben, B.; Dubovik, O.; Lin, S.-J. Sources and distributions of dust aerosols simulated with the GOCART model. *J. Geophys. Res. Atmos.* **2001**, *106*, 20255–20273. [\[CrossRef\]](#)
51. Löffler, M.; Brinkop, S.; Jöckel, P. Impact of major volcanic eruptions on stratospheric water vapour. *Atmos. Chem. Phys.* **2016**, *16*, 6547–6562. [\[CrossRef\]](#)
52. Joshi, M.; Jones, G. The climatic effects of the direct injection of water vapour into the stratosphere by large volcanic eruptions. *Atmos. Chem. Phys.* **2009**, *9*, 6109–6118. [\[CrossRef\]](#)
53. Schmidt, A.; Leadbetter, S.; Theys, N.; Carboni, E.; Witham, C.S.; Stevenson, J.A.; Birch, C.E.; Thordarson, T.; Turnock, S.; Barsotti, S. Satellite detection, long-range transport, and air quality impacts of volcanic sulfur dioxide from the 2014–2015 flood lava eruption at Bárðarbunga (Iceland). *J. Geophys. Res. Atmos.* **2015**, *120*, 9739–9757. [\[CrossRef\]](#)
54. Pattantyus, A.K.; Businger, S.; Howell, S.G. Review of sulfur dioxide to sulfate aerosol chemistry at Kilauea Volcano, Hawai‘i. *Atmos. Environ.* **2018**, *185*, 262–271. [\[CrossRef\]](#)
55. Heard, I.P.; Manning, A.J.; Haywood, J.M.; Witham, C.; Redington, A.; Jones, A.; Clarisse, L.; Bourassa, A. A comparison of atmospheric dispersion model predictions with observations of SO<sub>2</sub> and sulphate aerosol from volcanic eruptions. *J. Geophys. Res. Atmos.* **2012**, *117*, D20. [\[CrossRef\]](#)
56. Budyko, M. *Climatic Changes. Translation by the American Geophysical Union*; Waverley Press, Inc.: New York, NY, USA, 1977.
57. Hofmann, D.J.; Solomon, S. Ozone destruction through heterogeneous chemistry following the eruption of El Chichon. *J. Geophys. Res. Atmos.* **1989**, *94*, 5029–5041. [\[CrossRef\]](#)
58. Deshler, T.; Anderson-Sprecher, R.; Jäger, H.; Barnes, J.; Hofmann, D.J.; Clemesha, B.; Simonich, D.; Osborn, M.; Grainger, R.; Godin-Beekmann, S. Trends in the nonvolcanic component of stratospheric aerosol over the period 1971–2004. *J. Geophys. Res. Atmos.* **2006**, *111*, D1. [\[CrossRef\]](#)
59. Yuen, D.A.; Scruggs, M.A.; Spera, F.J.; Zheng, Y.; Hu, H.; McNutt, S.R.; Thompson, G.; Mandli, K.; Keller, B.R.; Wei, S.S.; et al. Under the surface: Pressure-induced planetary-scale waves, volcanic lightning, and gaseous clouds caused by the submarine eruption of Hunga Tonga-Hunga Ha‘apai volcano. *Earthq. Res. Adv.* **2022**, *2*, 100134. [\[CrossRef\]](#)
60. Aiuppa, A.; Bonfanti, P.; Brusca, L.; D’alessandro, W.; Federico, C.; Parello, F. Evaluation of the environmental impact of volcanic emissions from the chemistry of rainwater: Mount Etna area (Sicily). *Appl. Geochem.* **2001**, *16*, 985–1000. [\[CrossRef\]](#)
61. Delmelle, P.; Stix, J.; Bourque, C.P.-A.; Baxter, P.J.; Garcia-Alvarez, J.; Barquero, J. Dry deposition and heavy acid loading in the vicinity of Masaya Volcano, a major sulfur and chlorine source in Nicaragua. *Environ. Sci. Technol.* **2001**, *35*, 1289–1293. [\[CrossRef\]](#)
62. Kloss, C.; Sellitto, P.; Renard, J.B.; Baron, A.; Bègue, N.; Legras Berthet, G.; Briaud, E.; Carboni, E.; Duchamp, C.; Duflot, V.; et al. Aerosol characterization of the stratospheric plume from the volcanic eruption at Hunga Tonga 15th January 2022. *Geophys. Res. Lett.* **2022**, *49*, 16. [\[CrossRef\]](#)
63. Li, C.; Cohen, R.C. Space-Borne Estimation of Volcanic Sulfate Aerosol Lifetime. *J. Geophys. Res. Atmos.* **2021**, *126*, e2020JD033883. [\[CrossRef\]](#)
64. Carr, J.L.; Horváth, Á.; Wu, D.L.; Friberg, M.D. Stereo Plume Height and Motion Retrievals for the Record-Setting Hunga Tonga-Hunga Ha‘apai Eruption of 15 January 2022. *Geophys. Res. Lett.* **2022**, *49*, e2022GL098131. [\[CrossRef\]](#)
65. Beirle, S.; Boersma, K.F.; Platt, U.; Lawrence, M.G.; Wagner, T. Megacity emissions and lifetimes of nitrogen oxides probed from space. *Science* **2011**, *333*, 1737–1739. [\[CrossRef\]](#) [\[PubMed\]](#)

**Disclaimer/Publisher’s Note:** The statements, opinions and data contained in all publications are solely those of the individual author(s) and contributor(s) and not of MDPI and/or the editor(s). MDPI and/or the editor(s) disclaim responsibility for any injury to people or property resulting from any ideas, methods, instructions or products referred to in the content.